Slope instabilities in Dolomieu crater, Réunion Island: From seismic signals to rockfall characteristics

Clément Hibert, Anne Mangeney, Gilles Grandjean, Shapiro Nikolai

Slope instabilities in Dolomieu crater, Réunion Island: From seismic signals to rockfall characteristics

C. Hibert,[1,2] A. Mangeney,[1,3] G. Grandjean,[2] and N. M. Shapiro[1]

Received 29 March 2011; revised 23 October 2011; accepted 25 October 2011; published 23 December 2011.

[1] The seismic signals of hundreds of rockfalls within Dolomieu crater, Piton de la Fournaise volcano, Réunion Island, have been analyzed to investigate a possible link between physical rockfall-generating processes and associated seismic signal features. Moreover, indirect observation of rockfalls via the seismic signals they generate can provide useful data for studying volcanoes and the temporal variations of their structure. An increase in the number of rockfall events and their volumes might be an indicator of structural weakness and deformation of the volcano associated with potential eruptive activity. The study focuses on a 10 month period following the 6 April 2007 crater floor collapse within Dolomieu crater, from May 2007 to February 2008. For granular flows a scaling law is revealed between seismic energy and signal duration. A semiempirical approach based on both analytical analysis and numerical simulation of these flows shows that a similar scaling law exists between the difference of potential energy computed for an event and its propagation times and also emphasizes the effect of local topography on this scaling law. Simulated and observed data were compared to evaluate the proportion of potential energy dissipated in the form of seismic waves and confirm a direct link between the seismic energy and potential energy of a given granular flow. The mean ratio of seismic to potential energy is of the order of 10^{-4}, comparable to the range of values observed in previous studies. A simple method based on these ratios is proposed to estimate the volumes of rockfalls from their seismic signal. Observed seismic energy and the frequency of rockfalls decreased at the beginning of the studied period and reached a stable level in July, thus suggesting a postcollapse relaxation time of Dolomieu crater structure of about 2 months from seismic signal analysis, which is confirmed by deformation data. The total rockfall volume over the study period is estimated to be 1.85 Mm^3.

Citation: Hibert, C., A. Mangeney, G. Grandjean, and N. M. Shapiro (2011), Slope instabilities in Dolomieu crater, Réunion Island: From seismic signals to rockfall characteristics, *J. Geophys. Res.*, *116*, F04032, doi:10.1029/2011JF002038.

1. Introduction

[2] The unpredictable nature and destructive power of rockfalls make fast and reliable in-situ measurements of their properties (i.e., volume, runout distance, location) extremely difficult. Consequently, remote seismic monitoring may be a useful tool for studying such phenomena. Seismic signals associated with rockfalls and other mass movements have been studied extensively in many geological contexts showing that over and above event detection, seismic signals can provide important information on the characteristics of the source (e.g., volume, duration, and location) [*Vilajosana et al.*, 2008; *Deparis et al.*, 2007; *Helmstetter and Garambois*, 2010] even though the signal may be difficult to interpret because of topographic effects.

[3] Large rockfall events (10^4 to 10^7 m^3) have been studied by *Norris* [1994], who focused on 14 rockfalls at three Cascade Range volcanoes. This study showed an approximately linear relationship between source volume and seismogram amplitude for five rockfalls having the same source area and descent paths at Mount St. Helens. *Rousseau* [1999] investigated the relationship between amplitude and duration for hundreds of rockfalls that occurred during the 1995 episode located within the Mahavel Cascade, on Réunion Island. A model was developed that directly provided the volume of the rockfall from the maximum amplitude of its associated seismic signal.

[4] *Surinach et al.* [2005] examined the seismic signal generated by the 1 June 2005 landslide at Laguna Beach (California) and explained the general spectrogram features as functions of flow dynamics and topography effects. More recently, *Deparis et al.* [2007] studied 10 rockfalls recorded between 1992 and 2001 on a seismological network deployed

[1]Institut de Physique du Globe de Paris, Equipe Sismologie, CNRS UMR 7154, Université Paris Diderot–Paris 7, Paris, France.
[2]Bureau des Recherches Géologiques et Minières, RNSC/RMT, Orléans, France.
[3]Natural Risks and CO_2 Storage Safety Division, Université Paris Diderot–Paris 7, Paris, France.

0148-0227/11/2011JF002038

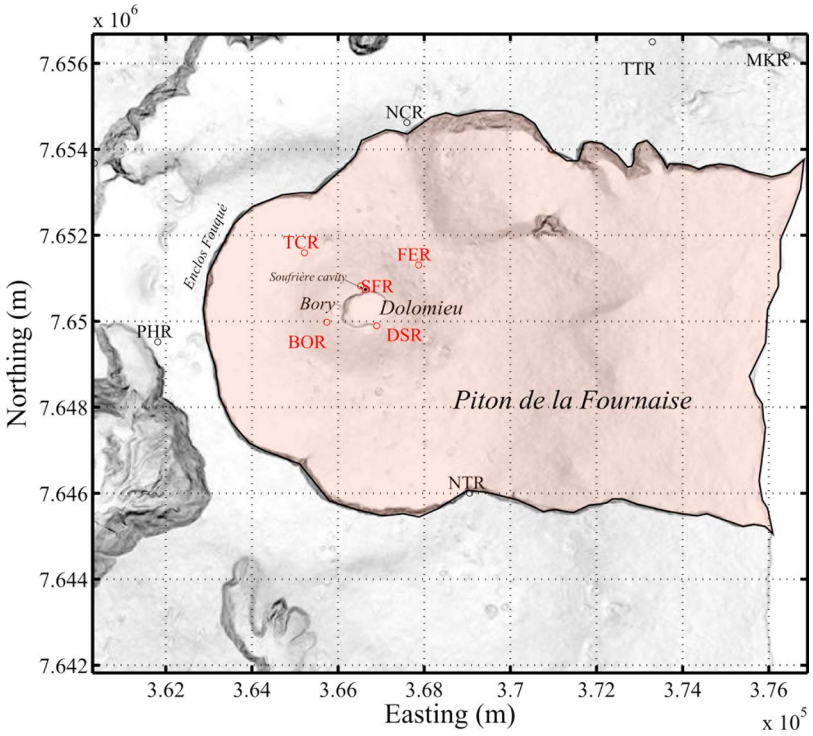

Figure 1. Station network of the Piton de la Fournaise volcano, Réunion island. Only the red stations are used in this study.

in the French Alps. They distinguished two seismic sources: one source corresponding to the detachment of the mass from the cliff and the other corresponding to the impact of the mass on the slope. They also compared rockfall parameters (fall height, runout distance, potential energy, volume) to the rockfall seismic magnitudes, duration, and energy, but found no relationships other than between the signal duration at an epicentral distance of 30 km and rockfall potential energy. The authors considered that this relationship corresponded to the control of the signal length by the event propagation phase. Finally, the ratio between seismic energy and potential energy computed for the 10 rockfalls gave values ranging from 10^{-3} to 10^{-5}.

[5] *Vilajosana et al.* [2008] investigated the seismic signal of a triggered rockfall in Montserrat (Catalonia). They too estimated the ratio between seismic energy and potential energy, but found a different value of about 2.5×10^{-1}. *Helmstetter and Garambois* [2010] studied the amplitude, seismic energy and duration distribution of thousands of rockfalls occurring on the Séchilienne slow motion landslide in the French Alps. They found that the distribution of rockfall seismic amplitudes followed a power law, which was not the case for signal amplitude and duration. Finally, a correlation was found between rockfall activity and landslide movement, as well as a weak but significant correlation between rockfall activity and rainfall.

[6] The previous studies emphasized the necessity to have seismic data on a large number of events and a substantial seismological network to better understand the linkage between seismic signal features and the intrinsic properties of rockfalls. The dense and permanent seismic network set up on the Piton de la Fournaise volcano, on Réunion Island, by the Observatoire Volcanologique du Piton de la Fournaise (OVPF) is particularly well suited for studying seismic signals generated by rockfalls. Furthermore, a major floor collapse that affected Dolomieu crater after a massive eruption in April 2007 [*Staudacher et al.*, 2009] considerably destabilized the crater walls and consequently increased the number of rockfalls affecting its edges, hence providing numerous seismological records generated by these events. These rockfalls involved individual meter-size blocks as well as larger volumes of up to several hundred cubic meters.

[7] In the present study we investigate the relationship between seismological records and rockfall activity that occurred near the summit of the volcano during two specific periods: a quiet period from February to July 2006, which preceded the 16 April 2007 crater floor collapse; and a second period from May 2007 to February 2008 following the crater floor collapse. No eruptions occurred during these periods. The aim of our study are threefold: (1) to determine what direct information can be obtained about rockfalls from their seismic signals (energy, signal duration), (2) to investigate whether rockfall properties such as volume can be estimated from these seismic signal parameters, and (3) to use rockfall properties estimated from seismic signals to investigate the temporal variations of the Piton de la Fournaise volcano and possible links between rockfall activity, flank deformation and environmental conditions.

[8] In this work, seismic signals were analyzed using signal processing techniques and features of seismic signals were compared to field observations and general knowledge of the rockfalls occurring near Dolomieu crater. In particular, seismic energy and signals duration were examined. A semiempirical approach based on analytical results and

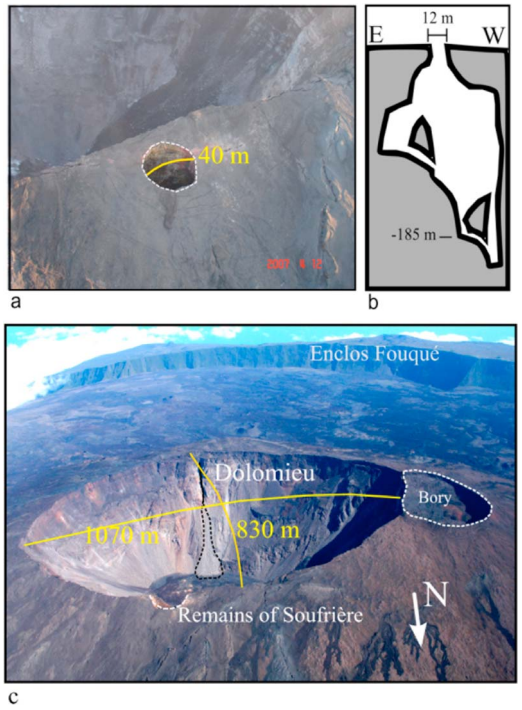

Figure 2. (a) Soufrière cavity as it was on 4 December 2007, a few days before it collapsed. (b) Schematic representation of Soufrière from *Rousseau* [1999]. (c) Aerial photograph of Piton de la Fournaise summit, Bory and Dolomieu craters, remains of Soufrière cavity, and highlighted (dotted black line) granular flow deposit.

numerical modeling was developed to estimate the proportion of rockfall energy dissipated in the form of seismic waves, thereby making it possible to estimate the collapsed volume from the observed seismic energy.

2. Context and Rockfall Qualitative Description

2.1. Geological Context: Piton de la Fournaise and the April 2007 Dolomieu Crater Floor Collapse

[9] The Piton de la Fournaise is an active volcano of Réunion Island. The eruptive center is located in a 8 km diameter large caldera named Enclos Fouqué. The present-day summit shows two collapsed structures named the Bory crater, which is currently inactive, and Dolomieu crater, within which numerous eruptions occur (Figure 1). Before the 2007 crater floor collapse, a 30 m wide, 40 m long, and 150 m deep pit crater, named Soufrière's cavity (Figure 2a), was located north and very close to Dolomieu crater. According to eye witnesses, this cavity formed during the 1964–1965 eruption and has enlarged by multiple edge collapses since then [*Rousseau*, 1999]. The cavity was explored in February 1985 by a team from the volcano observatory and members of the police force. A schematic representation of this cavity was made (Figure 2b). Prior to the April 2007 crater floor collapse, most of the rockfall observed close to the Piton de la Fournaise summit occurred within this cavity. The activity of Piton de la Fournaise is characterized by fissure eruptions fed by a magma reservoir located at about sea level [*Fukushima et al.*, 2005; *Peltier et al.*, 2007]. Since 1998, Piton de la Fournaise has been characterized by intense volcanic activity with 2 to 4 eruptions per year. Some of these eruptions occur in Dolomieu crater (Figure 1) contributing to the progressive filling of Dolomieu crater by accumulation of pahoehoe lava flows. Total filling of Dolomieu crater was attained with the August 2006 to January 2007 summit eruption [*Michon et al.*, 2007]. A major eruption, located 7 km east-southeast of the summit along a 1 km eruptive fissure started on 2 April 2007 at 06:00 GMT [*Staudacher et al.*, 2009]. Eruption intensity was very high, with lava fountains reaching a height of 100 to 150 m. This eruption led to the largest historical crater floor collapse observed at Piton de la Fournaise. The collapse was first recognized in the afternoon of 6 April. The initial collapse enlarged to about the size of the preexisting Dolomieu structure (870 m wide in north-south orientation and 1030 m long in east-west orientation), and deepened to about 340 m [*Urai et al.*, 2007]. Soufrière cavity was mostly destroyed by the collapse, and now only half of it remains (Figure 2c). The average slope angle of the inner crater walls is now about 40°, but with subvertical angles at certain locations, especially at the west-northwest edge of the crater beneath the Bory crater and former Soufrière cavity. Moreover, the edges of the crater expose highly fractured intercalated lavas and thin pyroclastics. According to *Staudacher et al.* [2009], the summit of the Piton de la Fournaise deflated significantly after Dolomieu collapse.

2.2. Qualitative Description of Rockfalls and Source Mechanisms

[10] During the time period investigated, two distinct types of rockfalls occurred. Before the 6 April 2007 collapse, the majority of rockfalls were recorded near the Piton de la Fournaise summit and occurred within the Soufriére cavity. Afterward rockfall activity was essentially limited to Dolomieu crater, because its inner walls were weakened and highly unstable.

2.2.1. Free-Fall-Type Rockfalls in Soufrière Cavity

[11] The geometry of the Soufrière cavity suggests that rockfalls there consist of two main phases in term of wave generation: the mass detaches from the cavity edges, then, after a free fall which may last approximately 4–5 s depending on cavity depth, the mass impacts the floor.

2.2.2. Granular Flow in Dolomieu Crater

[12] Since the crater floor collapse of 6 April 2007, numerous rockfalls have been detected by the seismic network and are still frequently observed today. Field observation of the rockfall deposits indicates that the dominant mechanism of mass wastage within Dolomieu crater is granular flow (Figure 2c). The deposits are completely unsorted and typically composed of material that ranges in size from fine (micrometric) grains to meter-size blocks. The deposit morphology suggests that the granular flows generally reach the bottom of the crater. Most of the flows result from destabilization of fractured rocks near the upper edges of the crater rim. From direct observation of several granular flows during field campaigns, the duration of these events is estimated to be several tens of seconds. The rockfalls of Dolomieu crater can be explained by three successive physical processes. The first is detachment of the mass from the cliff. The detached mass then impacts the slopes of the

inner crater wall after a short free fall and breaks up into block-rich granular material. Finally, the mass of rock fragments flows downslope over earlier deposits and comes to rest at the crater floor. This last phase of the rockfall process has the longest duration because of the lengths of the slopes, which can reach 500 m. The question we address is whether these different physical processes can be distinguished in the seismic signals generated.

3. Observations

3.1. Seismic Signals

[13] Seismic signals were studied from the continuous data records relating to 1706 rockfalls registered from May 2007 to February 2008 at four short-period stations (equipped with Lennartz L4C 1 Hz seismometers) of the OVPF seismological network. The stations used were BOR, DSR (later renamed to DSO), TCR, and FER (Figure 1). Forty-six rockfalls that occurred before the crater floor collapse, i.e., from February 2006 to January 2007, were also studied. For this precollapse period, data recorded at SFR station were also used. Rockfall signals are registered and manually identified every day at the observatory. Signal shape, duration and frequency content are used to discriminate rockfall seismic signal from others (Figure 3). A subset of the rockfall seismic signal was selected according to two criteria: (1) detection first at station BOR or DSR to ensure that the event took place in Dolomieu crater, and (2) detection by all four stations.

[14] The distances from the center of the crater to stations SFR, DSR, BOR, TCR, and FER are 300, 500, 800, 1800, and 2100 m, respectively, taking into account the topography. The distance between station SFR and Soufrière cavity was less than 50 m. Changes in the network during the period under study occurred when station SFR fell into Dolomieu crater with the collapse of Soufrière cavity, and station DSR, also threatened by the collapse, was moved 100 m back from the crater and renamed DSO. Consequently, it was not possible to use station SFR data for the period following the crater floor collapse.

[15] The signal sampling frequency is 100 Hz. The entire signal frequency power spectra was computed using the classical fast Fourier transform and the autoregressive Yule-Walker method [*Leonard and Kennett*, 1998]. Spectrograms were computed using a short-time Fourier transform with a moving 2.56 s (256 sample) window and an overlap of 95%. The combined observation of seismograms, frequency-power spectra, and spectrograms made it possible to distinguish several classes of events: volcanotectonic earthquakes, granular flow-type rockfalls and free-fall-type rockfalls within the Soufrière cavity (Figure 3).

3.1.1. Volcanotectonic Earthquakes

[16] These events are generated by the fracturing of rock induced by magma and gas movement within the volcano [*McNutt*, 1996; *Zobin*, 2003]. The associated seismic signal (Figure 3a) is characterized by an impulsive onset clearly visible on the seismic signal and of relatively short duration, i.e., generally less than 40 s. The spectrogram (Figure 3b) has a specific shape with a sharp amplitude increase followed by an exponential decay of the frequency content with time. Volcanotectonic (VT) earthquakes are characterized by a wide frequency band which can reach a maximal value of about 30 Hz which slightly decreases with distance between the event and the station (Figure 3c). The frequency spectrum shows several peaks, and P and S waves can normally be identified.

3.1.2. Rockfalls: Granular Flows

[17] Seismic signals generated by granular flows have been observed since the 2007 crater collapse. The seismic signal shows an emergent onset and a long duration ranging from 50 to more than 200 s. The duration is 120 s for the example shown in Figure 3d. In general, no clear peak amplitude is observed on the seismograms, and P and S waves cannot be distinguished. This is probably due to the complexity of the source mechanism and also to a dominance of surface waves in the rockfall-generated seismic signal [*Rousseau*, 1999; *Deparis et al.*, 2007]. The frequency band, as presented in Figure 3f, ranges from 2 to 10 Hz and is centered at 5 Hz, similar to the range observed for granular flows at Merapi volcano [*Ratdomopurbo and Poupinet*, 2000] and at Montserrat [*Calder et al.*, 2002; *Luckett et al.*, 2002]. *Vilajosana et al.* [2008] and *Bessason et al.* [2007] both observed a higher frequency band for a rockfall-generated seismic signal that reached 50 Hz, but the seismic stations were located within 100 m of the seismic sources, whereas our closest station, DSR(O), is 600 m from the crater center. The impact of source-receiver distance on the observed frequency bands is likely due to the intrinsic attenuation of high-frequency signals [*Aki and Richards*, 1980] favored in our case by the loosely compacted, course granular substrate [*Ferrazzini et al.*, 1991]. The spectrogram for granular flows (Figure 3e) reveals a cigar shape, similar to the shape observed by *Surinach et al.* [2005], which generally reflects a linear frequency decay with time. These spectrogram features are observed consistently at all stations recording granular flow. Consequently, this specific spectrogram shape is probably due to the source mechanism rather than the seismic wave propagation path. No clear phases are seen in the seismic signal, i.e., the three physical processes described earlier cannot be distinguished on the seismograms. Nevertheless, the geomorphology of the inner Dolomieu crater slopes and the fact that seismic signal duration and observed granular flow propagation time are very close suggests that most of the seismic signal is generated by granular material flowing along the crater slopes. Thus, as observed by *Deparis et al.* [2007], the propagation of granular flow seems to be the physical process that controls the signal duration. The fracturing of the mass after its free fall following detachment from the cliff may contribute to seismic signal generation, but this phase is not distinguishable in the seismic data.

3.1.3. Rockfalls: Free-Fall-Type Rockfalls Within the Soufrière Cavity

[18] The seismic signal associated with free-fall-type rockfalls (Figure 3g) has an impulsive onset and short duration, similar to the VT events. Figures 3h and 3i show that the frequency band observed at distant stations (here TCR) contains slightly higher frequencies than those observed for granular flows, with a central frequency around 7 Hz. It also exhibits much lower frequencies than those observed for VT seismic signals. Nevertheless, high frequencies up to around 40 Hz are observed and appear less attenuated at station SFR (Figures 3h and 3i). This station was very close (about 50 m) to the Soufrière cavity, thus revealing the high attenuation of high frequencies with propagation distance. The signals

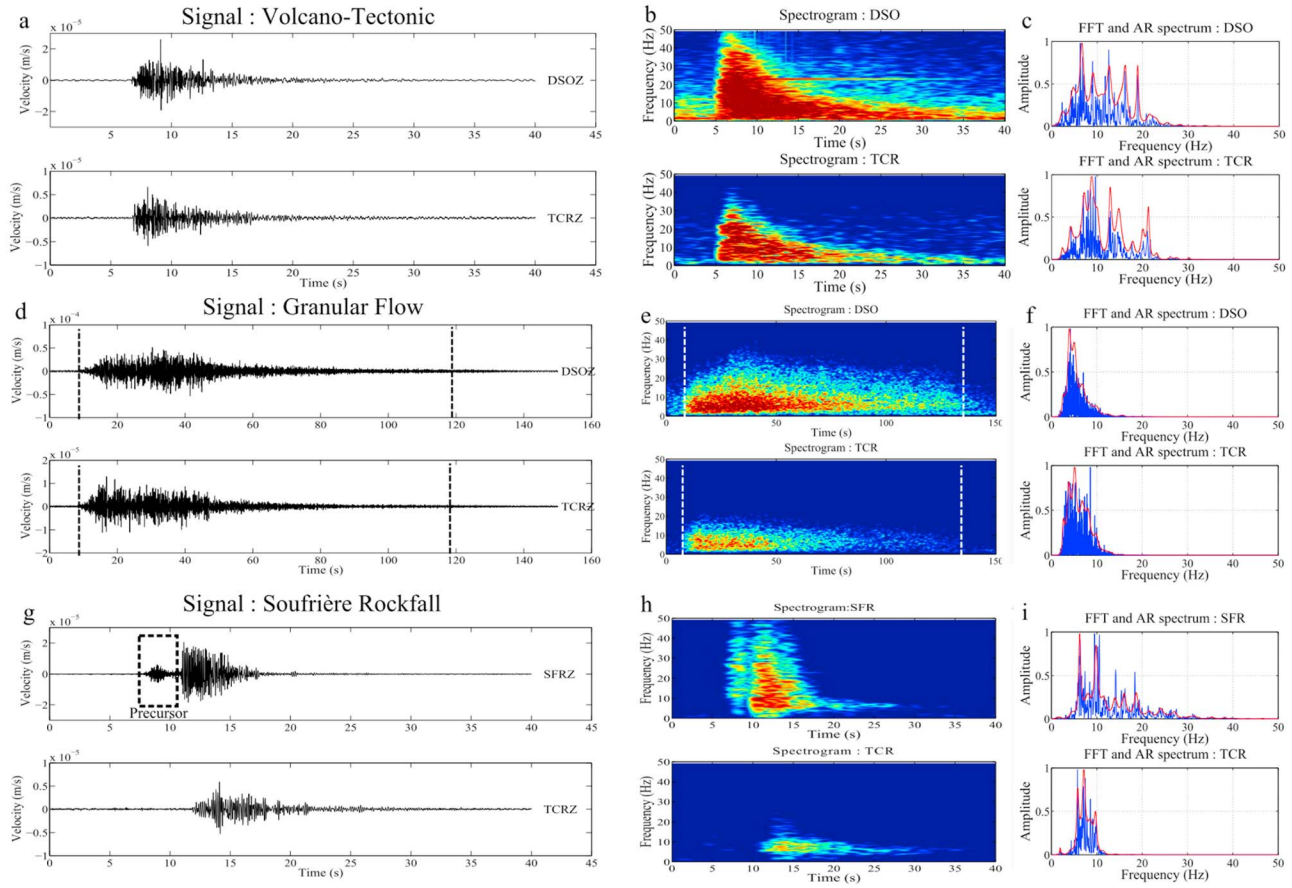

Figure 3. (a) Seismic signal, (b) spectrogram, and (c) fast Fourier transform (FFT) (blue) and AR (red) frequency power spectrum for volcanotectonic earthquake; (d) seismic signal and picked times, (e) spectrogram, and (f) FFT (blue) and AR (red) frequency power spectrum for a granular flow; and (g) seismic signal, (h) spectrogram, and (i) FFT (blue) and AR (red) frequency power spectrum for a free fall of rock in Soufrière cavity.

recorded at station SFR have a characteristic shape, with a lower-amplitude precursor. This precursor appears only on signal recorded at SFR station because of the attenuation of the higher frequency and the scattering of seismic waves. The two parts of the signal could possibly be related to the two physical processes described in section 2 for the Soufrière cavity rockfalls; i.e., the first part of the signal could be linked to the rebound of the edge from which the falling mass became detached, and the second part could result from the impact of the mass on the Soufrière cavity floor. The time interval between the first and second parts of the signal is about 4 s, which roughly corresponds to the time of fall from the detachment zone to the Soufrière cavity floor. This tends to support our interpretation. It is important to note that the maximum amplitude of the signal for these rockfalls is generated by the impact on the cavity floor and not by the block's detachment. Because maximum amplitude is a common parameter used in studying rockfall-generated seismic signals, it is critical to know which physical process corresponds to the peak.

3.2. Seismic Energy and Signal Duration: Scaling Laws

[19] We investigated attributes of the seismic signals of the rockfalls occurring after the 6 April 2007 crater floor collapse that could help us deduce information on the granular flow properties. We focused in particular on two parameters: signal duration and seismic energy. The few field observations of rockfalls show that the duration of the seismic signal corresponds mostly to the duration of the granular flow. Moreover, duration is a very simple parameter to obtain from seismic signals, and on the basis of existing literature, it gives the best correlation with various rockfall characteristics such as runout, volume and potential energy [*Deparis et al.*, 2007]. Rockfall duration may also provide significant information on volcanic activity [*Calder et al.*, 2005; *Zobin et al.*, 2008]. In this study we prefer to examine seismic energy rather than peak amplitude because the latter does not incorporate the complex dynamics of the granular flow source. Furthermore, as discussed in section 3.1, peak amplitude is difficult to determine from the seismic signal generated by granular flows.

[20] The duration of each event was picked manually. The emergent onset and the very slow decrease in amplitude of these signals made it difficult to accurately pick the event duration. To ensure a good pick onset and final times were observed on several frequency bands and on the spectrograms. The onset time was picked when the amplitude clearly emerges from the noise, and the spectrogram shows

an energy increase in the frequency band superior to 2 Hz. The final time was picked when the signal becomes indistinguishable from the noise, and when the energy on the spectrogram has reached the level observed prior to the onset (Figures 3d and 3e). This picking method is fairly subjective, and our results may not be very accurate, with errors that may exceed 1 s. However, as rockfall seismic signals have durations of tens of seconds, the relative error does not greatly affect the durations extracted from the signals used in this study. These errors will become more problematic if precise rockfall locations are to be determined in the future.

[21] A first approximation of the energy dissipated in the form of seismic surface waves, assuming an isotropic homogeneous propagation medium and a point-force source [*Kanamori and Given*, 1982; *Eissler and Kanamori*, 1987; *Dahlen*, 1993], can be obtained using the relationship used by *Vilajosana et al.* [2008] assuming that surface waves dominate the seismic signals:

$$Es = \int_{t_1}^{t_2} 2\pi r \rho h c \, u_{env}(t)^2 e^{\alpha r} dt \tag{1}$$

with

$$u_{env}(t) = \sqrt{u(t)^2 + \mathrm{Ht}(u(t))^2} \tag{2}$$

where t_1 and t_2 are the picked onset and final times of the seismic signal, respectively, r is the distance between the event and the recording station, h is the thickness of the layer through which surface waves propagate, ρ is the density of the ground, c is the phase velocity of the seismic waves, u_{env}(t) is the amplitude envelope of the seismic signal (here the ground velocity) obtained using the Hilbert transform (Ht), and α is a damping factor that accounts for anelastic attenuation of the waves [*Aki and Richards*, 1980]. This damping factor is frequency dependent and was computed as

$$\alpha = \frac{f\pi}{Qc} \tag{3}$$

We impose a frequency f = 5 Hz, because this is the center of the frequency band where most of the energy is observed for granular flows (Figure 3f). On the basis of the typical phase velocity for surface waves in volcanic areas [*Ferrazzini et al.*, 1991; *Brenguier et al.*, 2007] and the significant fracturing of the upper layers of the crater walls, we assume a velocity of c = 800 m/s and a quality factor accounting for the attenuation of seismic wave Q = 50, which is within the range of the values obtained by *Koyanagi et al.* [1992] for Kilauea volcano. We assume a rock density of ρ = 2000 kg m^{-3}, a classical value for volcanic rock. Because the events could not be specifically located, r is assumed to be the distance between the stations and the center of the crater. The thickness h = 160 m was taken as one wavelength of Rayleigh waves with a frequency peak of 5 Hz propagating with the velocity chosen.

[22] Seismic energy (E_s) was plotted as a function of the seismic signal duration (t_s) for each rockfall event from May 2007 to February 2008 in order to study the relationship between these two quantities (Figure 4). The seismic energy ranges from 10^3 to 10^7 J, covering 4 orders of magnitude. The duration varies from a minimum of 10 s to a maximum of about 200 s.

[23] Least squares regression lines are fitted to the points clouds for each month. The corresponding regression coefficients β_s represent the slope of the regression line in the log-log domain. They are plotted for each month and each station in Figure 5a. The mean coefficients are plotted in Figure 5b with their corresponding standard deviations. R^2 and p values are plotted in Figures 5c and 5d, respectively. The β_s coefficients have a value between 1 and 2 and are reasonably stable over time. The mean value of the coefficients over the four stations is 1.52. The corresponding mean standard deviation is 0.48. Its minimum is reached in August with a value of 0.1. The coefficient of determination R^2 varies greatly from 0.1 to 0.7, corresponding to a very poor to strong relationships between seismic signals duration and seismic energy, respectively. Inherent variability caused by the errors made in picking signal duration and the approximations made in the energy computation have a substantial impact on the coefficients β_s. Nevertheless, it is important to note that the closer the regression coefficients to $\beta_s = 2$, the higher the R^2 coefficients. Also, R^2 coefficients are higher for data observed at station DSR which is the closest to Dolomieu crater. Hence, seismic waves recorded at DSR are less prone to attenuation or scattering and may better correlate with the source properties. The p values are always less than 0.05. Thus it is possible to infer that a relationship between E_s and t_s is likely to exist in the form of

$$E_s = A t_s^{\beta_s} \tag{4}$$

where β_s are the coefficients of the regression lines.

4. Interpretation From Granular Flow Models

[24] A scaling law has been found between seismic energy and signal duration for the granular flows occurring in Dolomieu crater. The question that had to be addressed concerns the origin of such a relationship and whether it is related to granular flow processes. We proposed an analysis based on granular flow models and focused on the propagation time and potential energy difference between the initial and final state of the granular mass involved.

4.1. Analytical Solution on an Inclined Bed

[25] Our first analysis is not an exhaustive and exact description of a realistic phenomena, but rather a simple way to understand the interconnection of the quantities involved. We examine the potential energy lost during a flow. Our model has been developed on the basis of theoretical and experimental work on granular material flowing over inclined planes [*Mangeney et al.*, 2000, 2010]. As shown previously, most mass wastage events are dominated by the phase where granular material flows down the slopes of the crater. Let us consider the simple case of a 2-D dry granular flow down along inclined plane of slope θ generated by the sudden release of a rectangular mass (Figure A1a). The seismic energy is part of the global energy lost during the motion of the granular mass from its initial to its final state. The energy lost during the flow process is

$$\Delta E = \left(E_{pf} + E_{cf}\right) - \left(E_{pi} + E_{ci}\right) \tag{5}$$

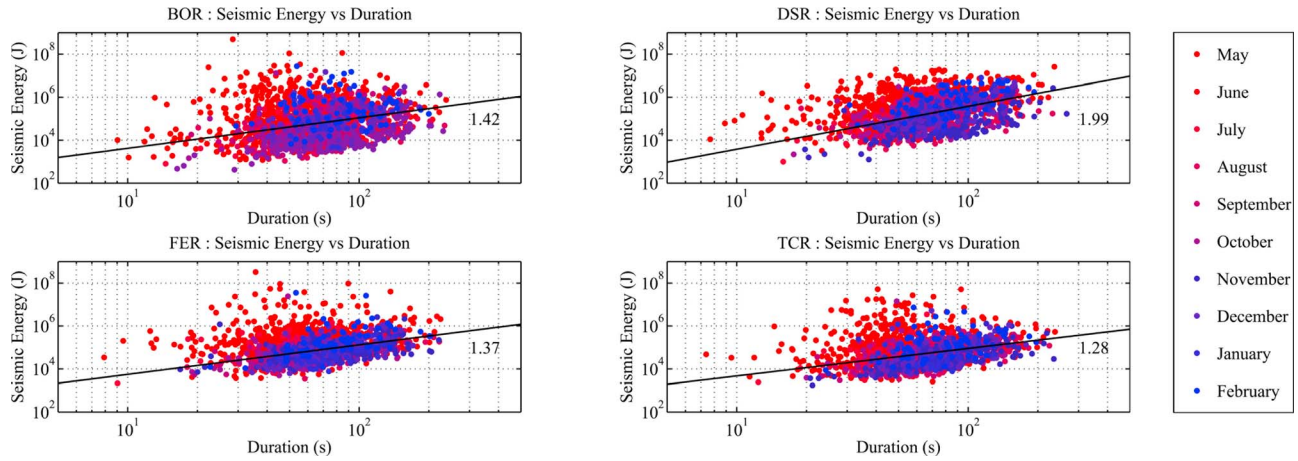

Figure 4. Seismic energy (E_s) as a function of signal duration for the 1706 recorded granular flows. Best fit regression lines and power law coefficients are given on each plot.

where E_p is the potential energy, E_c is the kinetic energy, and the subscripts i and f denote the initial and final states, respectively. As the mass has no initial velocity and is ultimately at rest:

$$E_{cf} = E_{ci} = 0$$

Therefore, the total energy dissipated during the flow is the potential energy lost:

$$\Delta E_p = mg\left(z_{Gf} - z_{Gi}\right) \tag{6}$$

where z_{Gf} and z_{Gi} refer to the final and initial vertical positions of the mass center respectively and m is the mass and g is the

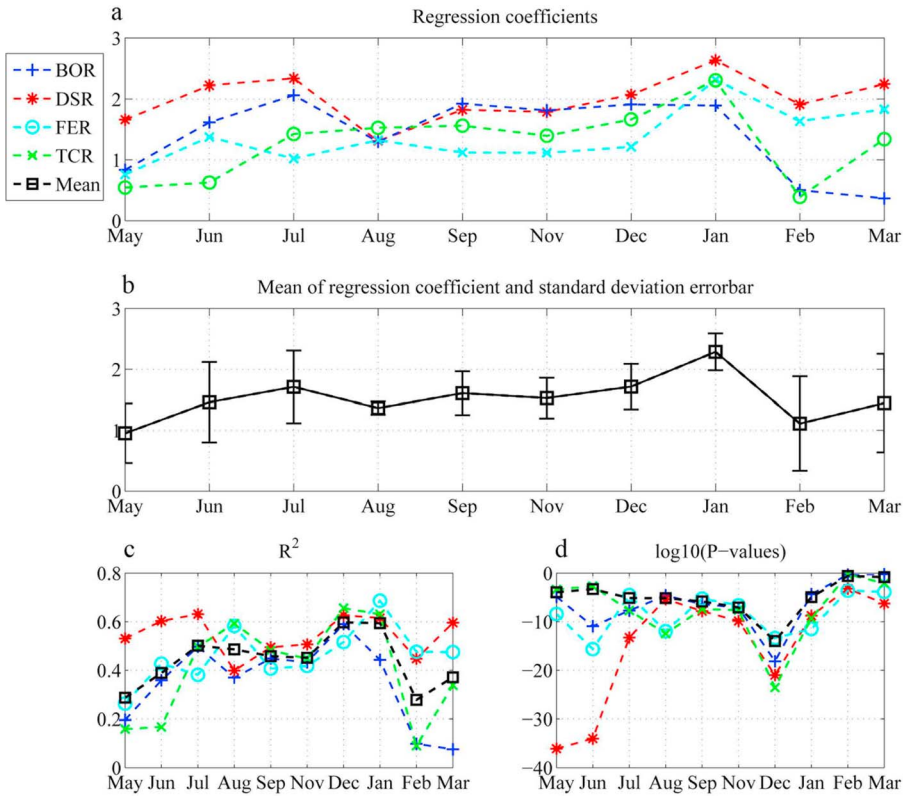

Figure 5. (a) Regression coefficients of the lines fitting point clouds for each month at the four stations, (b) mean regression coefficient per month, (c) R^2 values from the computation of the regression coefficients for each month at each of the four stations, and (d) log of the p values from the computation of the regression coefficients for each month at each of the four stations.

gravitational acceleration. The details of the analytical solutions are presented in Appendix A. The resulting expression of the difference of potential energy of a granular flow on a flat slope is

$$\Delta E_p = mg\left[\frac{-h_0\cos\theta}{2} + \frac{1}{3}(\tan\alpha\cos\theta - \sin\theta)r_f + \frac{1}{3}\left(\tan\alpha\cos\theta + \frac{\sin\theta}{2}\right)r_0\right] \quad (7)$$

where h_0 is the initial height of the mass (i.e., the thickness), r_0 its initial length, r_f the final runout distance, α the average angle of the final deposit and θ the average slope angle (see Figure A1 in Appendix A). *Börzsönyi et al.* [2008] and *Mangeney et al.* [2010] have shown experimentally that the average angle of the deposit with respect to the horizontal plane for glass beads, i.e., $\theta + \alpha$, is very close to the friction angle δ of the material involved. Assuming this also applies to our case, we can express the following equation between the friction angle δ, the slope angle θ, and the angle α:

$$\delta = \alpha + \theta \quad (8)$$

Furthermore, *Mangeney et al.* [2010] have found empirically that the propagation time of a granular flow t_f is a function of h_0:

$$t_f = 2\sqrt{\frac{kh_0}{g\cos\theta}}\frac{1}{\tan\delta - \tan\theta}; \quad (9)$$

thus,

$$h_0 = t_f^2\frac{1}{4k}\left[g\cos\theta(\tan\delta - \tan\theta)^2\right] \quad (10)$$

where the coefficient k is equal to 0.5. This solution is derived from experimental results and analytical results for granular collapse over inclined bed. However in our specific context, the granular flows generally reach the bottom of the crater and stop there so that the run out is imposed by the position of the crater floor (Figure A1b). In this case r_f is roughly constant and set equal to L. Let us assume that $L \gg h_0$ and $L \gg r_0$ so that the terms involving h_0 and r_0 are negligible. Typical values for L are around 500 m while h_0 and r_0 are of the order tens of meters. Consequently, the h_0 and r_0 terms account for less than 10% of the value of the difference of potential energy. As a result equation (7) becomes

$$\Delta E_p = mg\left(\frac{L}{3}(\tan\alpha\cos\theta - \sin\theta)\right) \quad (11)$$

[26] The initial mass m can be expressed as a function of the initial parameters h_0 and r_0, the initial width of the mass w_0, and the density ρ:

$$m = \rho h_0 r_0 w_0$$

[27] Consequently, equation (11) becomes

$$\Delta E_p = \rho h_0 r_0 w_0 g\left(\frac{L}{3}(\tan\alpha\cos\theta - \sin\theta)\right) \quad (12)$$

[28] Combining equations (10) and (12), we obtain

$$\Delta E_p = t_f^2\left[\frac{L\rho r_0 w_0 g^2}{4k}\left(\frac{1}{3}(\tan\alpha\cos\theta - \sin\theta)\right)\cdot\left(\cos\theta(\tan\delta - \tan\theta)^2\right)\right] \quad (13)$$

Therefore, the difference in potential energy varies as a function of the stopping time of the granular flow:

$$E_p = B(r_0, w_0)t_f^{\beta_p} \quad (14)$$

with exponent $\beta_p = 2$, which is slightly higher than that observed from the seismic data. In an identical context (δ, θ, L, and ρ constant), parameter B is a function of only the initial mass geometry parameters r_0 and w_0. Because r_0 and w_0 reach at most tens of meters, they should theoretically introduce a maximum dispersivity of the order of 10^2 on the computed potential energy. Despite the relative simplicity of this analytical development, we do find a relationship (14) between potential energy and event duration compatible with what is observed between seismic energy and signal duration.

4.2. Numerical Modeling on Real Topography

[29] To investigate the existence of a relationship between potential energy and event duration using a more realistic approach, and to assess the role of local topography on the scaling law, we carried out simulations of granular flows. We used the SHALTOP numerical model that describes dry granular flows over a complex 3-D topography [*Bouchut et al.*, 2003; *Bouchut and Westdickenberg*, 2004; *Mangeney-Castelnau et al.*, 2005; *Mangeney et al.*, 2007]. This model is based on a depth-averaged thin layer approximation (the flow is assumed thin compared to its longitudinal extent) and takes into account a Coulomb-type friction law. It describes the change of flow thickness with time $h(x, y, t)$ in the direction normal to the topography and the depth-averaged velocity of the flow $u(x, y, t)$ along the topography $z = b(x, y)$ where (x, y, z) are the coordinates in a Cartesian reference frame. This model deals with the full tensor of terrain curvature. SHALTOP has successfully reproduced experimental granular flows [*Mangeney-Castelnau et al.*, 2005; *Mangeney et al.*, 2007] and natural landslides [*Lucas and Mangeney*, 2007; *Kuo et al.*, 2009; *Mangold et al.*, 2010; *Favreau et al.*, 2010; *Lucas et al.*, 2011]. Moreover, *Favreau et al.* [2010] have shown that simulation of seismic waves generated by a landslide with SHALTOP coupled with a wave propagation model can be used to calculate an appropriate source function for the landslide. Because the main issue in granular flow modeling is the lack of full understanding of the mechanical behavior of a flow, we choose here the simplest friction law $\mu = \tan\delta$, where δ is the friction angle and μ is the friction coefficient. This friction coefficient can be considered a measure of the mean dissipation during flow [*Mangeney et al.*, 2010].

[30] The 2-D numerical simulations were run on three profiles extracted from a digital elevation model (DEM) constructed from photographs taken during a field program in October 2009 [*Hibert et al.*, 2010].The profiles were selected from the area where, according to field observations, most of the rockfalls occurred (see Figure 6 for their locations and

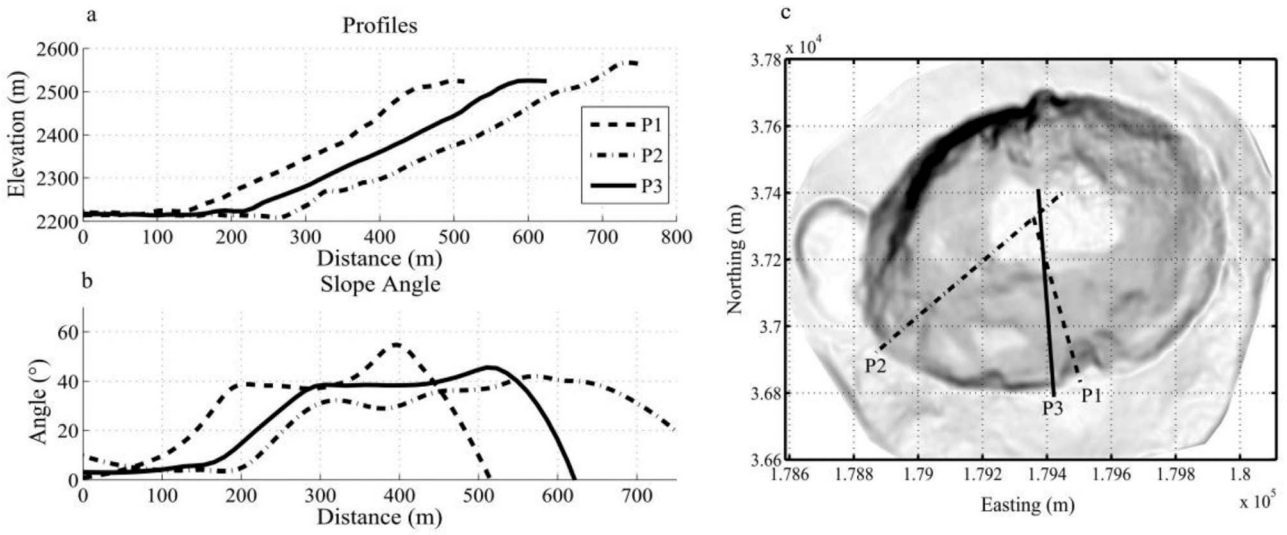

Figure 6. (a) Profiles used for granular flow simulations, (b) slope angles of the corresponding profiles, and (c) location of the profiles.

slope angles). The friction angle δ was calibrated from propagation times, i.e., δ was adjusted so that simulated flow durations were in the range of the observed seismic signal durations. We used a value of $\delta = 35°$. This friction angle value is approximately the slope of the granular flow deposits observed in Dolomieu crater. Note that for flow over an inclined bed, changes in δ affect coefficient B in equation (14) but do not affect the exponent β_p. Fifty simulations were conducted on each profile, with randomly generated volumes ranging from 5 to 400 m^3 as suggested from field observations. Indeed, most of the events seem to be in that range although some events could have volumes of up to around 10^3 m^3.

[31] As shown in Figure 7, the initial mass geometry is, in reality, released from rest on the topography (Figure 7a). This mass spreads over the slope as a thin layer of granular material flowing down to the crater floor to form a bulge at the bottom of the slope while material is still flowing from the departure zone (Figure 7b). All the material eventually stops at the bulge to form a deposit (Figure 7c). Note that simulations using SHALTOP do not take into account a possible material recharge of the granular flow from erosion processes and/or successive collapses from the departure zone. Consequently, real granular flow durations may sometimes be longer than those simulated [*Mangeney et al.*, 2010].

[32] The difference in potential energy for each event was calculated using SHALTOP. Ending state time was determined when significant changes no longer appeared in the calculated potential energy. The results for each profile are plotted in a log-log representation and each point cloud is fitted by a least squares regression line (Figure 8). The dispersion of the potential energy values around the regression line, cover 2 orders of magnitude as expected theoretically from the dispersion of the geometrical properties of the mass (h_0, r_0, and w_0). The calculated regression coefficients β_p are presented in Figure 8. The scaling law is similar to the one computed from seismic energy. The β_p values are 1.70 for profile P1, 1.36 for profile P2, and 1.88 for profile P3. The coefficients of determination R^2 are 0.55, 0.52, and 0.58, respectively. The p values are 4.9×10^{-5}, 2.6×10^{-3}, and 1.4×10^{-5}, respectively. The β_p values are consistent with the analytical solution $\beta_p = 2$ for granular flow over an inclined bed. It seems that increasing the rugosity of the topography tends to decrease values of the coefficients. Although the differences found are relatively small, the highest coefficient was for profile P3 which is the smoothest profile and the lowest coefficient was for profile P2 which has the roughest topography (Figure 6b). However, they vary very slightly and more simulations have to be made to study the linkage between the behavior of these coefficients and the topography rugosity.

5. Estimating Rockfall Volumes From Seismic Signals

[33] We have seen that scaling laws relating energy and time are similar whether obtained from an analysis of seismic data or from simulations of granular flow. This point, in addition to the observed fact that the duration of a rockfall and that of the associated seismic signal are similar, suggests that the seismic energy is somehow proportional to potential energy lost during the rockfall event. Some authors have quantified the proportion of potential energy dissipated in the form of seismic energy for the case of rockfalls or landslides. *Deparis et al.* [2007] found E_s/E_p ratios ranging from 10^{-3} to 10^{-5} for ten rockfalls recorded by a regional seismological network in the Alps with volumes ranging from 2×10^3 to 1.75×10^6 m^3. They consider the large variations in the ratio values to reflect the highly varied geotechnical conditions of the different sites.

[34] A smaller rockfall (V = 70 m^3) was studied by *Vilajosana et al.* [2008]. In this case, the seismological network formed by two stations was as close as a few tens of meters to the source. The E_s/E_p ratio was found to be 0.25. The ratio values from these two studies are very different and denote the strong influence of a site's seismological properties as well as of the type of rockfall. In our study,

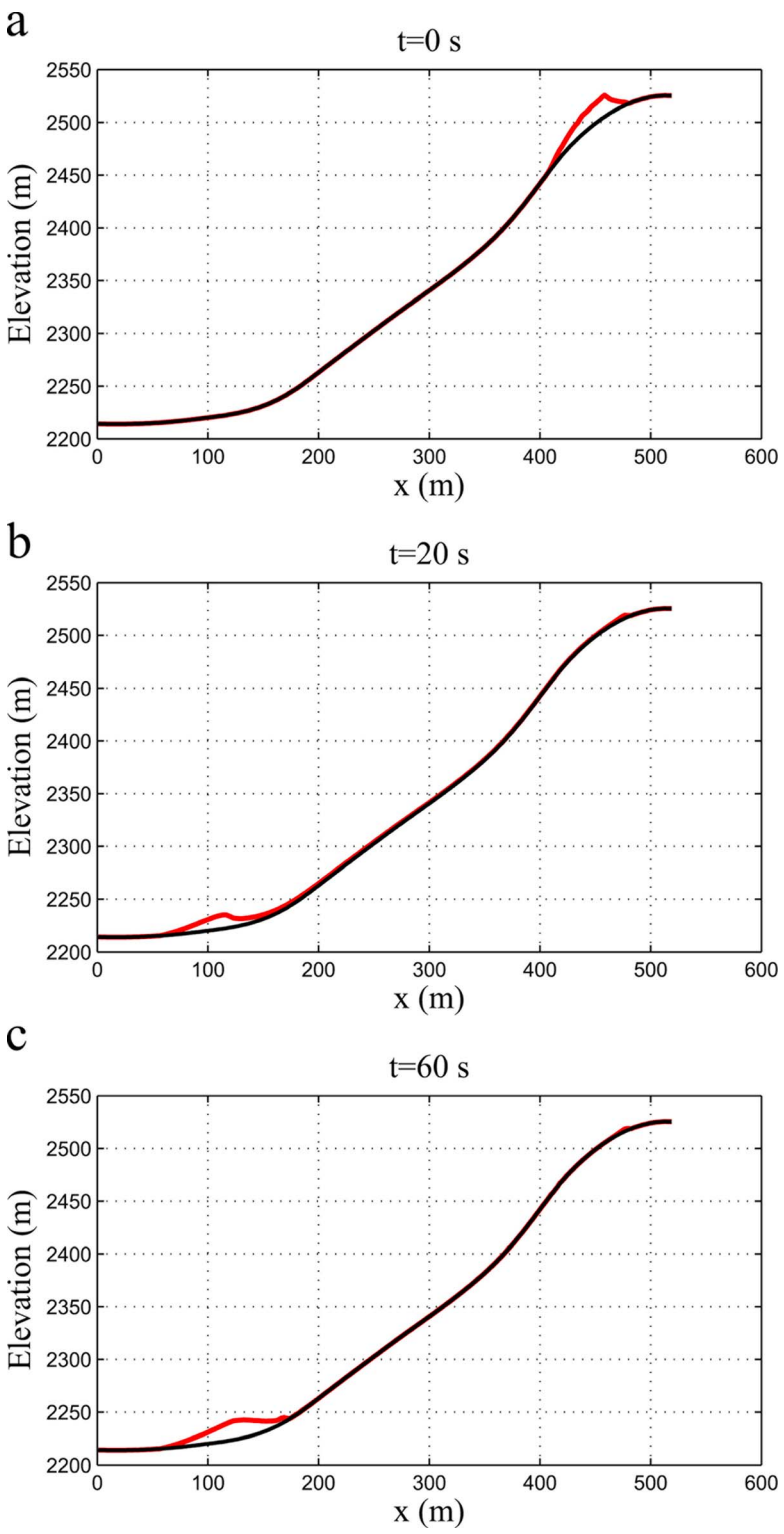

Figure 7. Position of granular mass at various times during a simulation: (a) initial position, (b) mass at time t = 20 s, and (c) mass at time t = 60.

both the nature of the rockfalls generated and the site geological conditions remain the same over the period studied.

5.1. Seismic to Potential Energy Ratio

[35] To assess the E_s/E_p ratios, the observed seismic energy data are compared to the simulated potential energy data. The observed and calculated point clouds are fitted by least squares regression lines. Then, for each month and each station, the difference between the simulated and observed regression lines is minimized, thereby giving directly the E_s/E_p ratio. The fitting process and results are shown in Figure 9 for October 2007, and the ratios are given in Table 1.

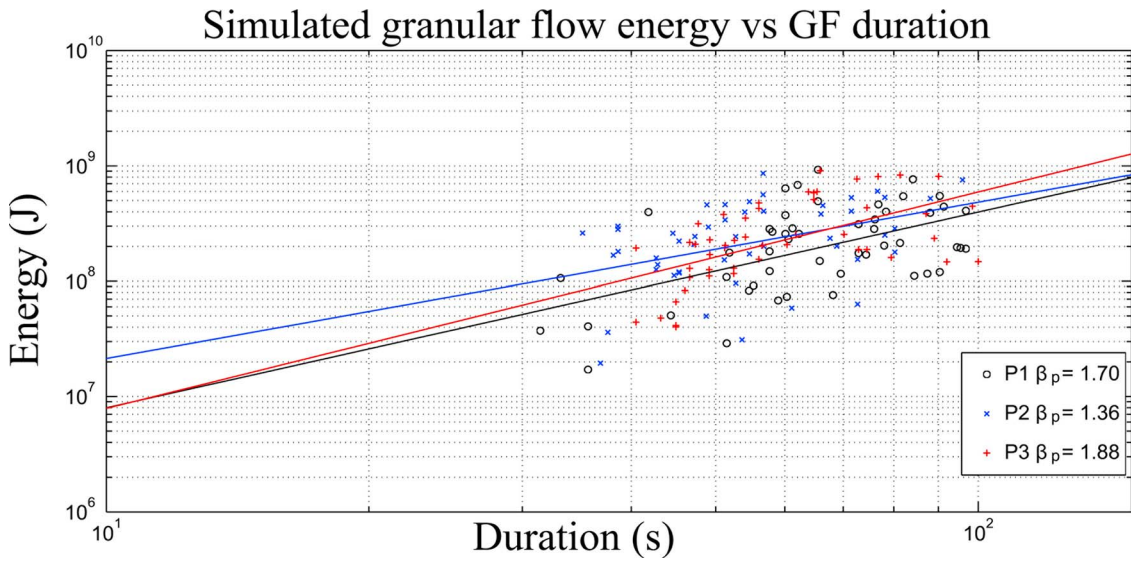

Figure 8. Difference of potential energy between initial and ending states of granular flows as a function of the flow duration for the 150 simulations made on the three profiles along with corresponding regression line coefficients.

[36] Table 1 shows that the ratios are roughly constant in both time and space, with values ranging from 10^{-5} to 10^{-3}. The ratio values are of the order of those found by *Deparis et al.* [2007]. It appears that ratios are the highest for months with high mean seismic energy generated by rockfall (May 2007 and February 2008 as presented in section 6). The high-energy rockfalls that occurred during these months may be able to transmit more energy in the form of seismic waves. The high seismic energy values also impact on the method by raising the mean of the seismic energy values and therefore the position of the regression lines. Spatial disparity is indicated by the lower mean ratio value at station TCR, which is possibly explained by our seismic energy computation assumption that the distance r traveled by the seismic waves is the topographic distance between the center of the crater and the station. The traveled path could however be much longer because seismic waves generated by granular flows are dominated mainly by surface waves and these could remain trapped in the highly fractured medium. For example, the presence of the Bory crater on the path followed by the seismic waves from the crater to station TCR could explain why this effect is the strongest at station TCR. Station FER appears to show a similar phenomenon, although to a lesser extent, possibly because of the lack of a structure like the Bory crater on the travel path from Dolomieu crater.

5.2. Volume Deduction

[37] Estimating rockfall volumes from the seismic signal is a difficult task considering the complexity of the physical processes involved and the number of parameters influencing

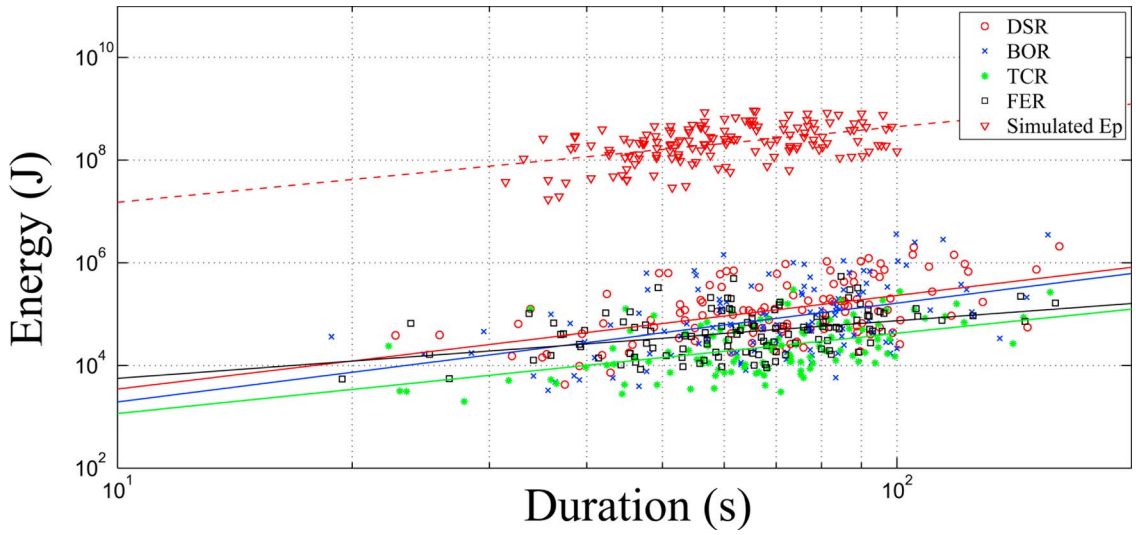

Figure 9. Simulated potential energy and observed seismic energy as a function of flow duration and corresponding best fit regression lines.

Table 1. E_s/E_p Ratios Computed From the Data Recorded at Stations BOR, DSR, TCR, and FER

	BOR	DSR	TCR	FER
May 2007	8.26×10^{-4}	2.78×10^{-3}	3.15×10^{-4}	1.27×10^{-3}
June 2007	5.99×10^{-4}	7.58×10^{-4}	1.76×10^{-4}	2.52×10^{-4}
July 2007	7.30×10^{-4}	1.19×10^{-3}	1.62×10^{-4}	3.11×10^{-4}
August 2007	1.80×10^{-4}	3.44×10^{-4}	8.25×10^{-5}	2.31×10^{-4}
September 2007	3.29×10^{-4}	4.74×10^{-4}	9.16×10^{-5}	1.81×10^{-4}
October 2007	4.18×10^{-4}	5.26×10^{-4}	1.08×10^{-4}	1.99×10^{-4}
November 2007	1.04×10^{-4}	2.13×10^{-4}	6.99×10^{-5}	2.16×10^{-4}
December 2007	5.26×10^{-4}	8.06×10^{-4}	1.46×10^{-4}	2.75×10^{-4}
January 2008	7.94×10^{-4}	8.62×10^{-4}	1.55×10^{-4}	1.80×10^{-4}
February 2008	1.41×10^{-3}	2.00×10^{-3}	3.34×10^{-4}	5.88×10^{-4}
Mean	5.91×10^{-4}	9.95×10^{-4}	1.64×10^{-4}	3.70×10^{-4}
Standard deviation	3.83×10^{-4}	8.07×10^{-4}	9.21×10^{-5}	3.37×10^{-4}

the seismic signal. A first attempt was made by *Rousseau* [1999] who used the maximum amplitude of the seismic signal to deduce the volumes of events occurring during the 1995 Mahavel rockfall episode on Réunion Island. Here we propose a different approach based on the energy ratios computed in section 5.1. These are used to obtain an estimate of the potential energy difference for each event and then to calculate their volume from the approach presented above. The seismic energy for each granular flow can thus be expressed as a function of the potential energy difference:

$$E_s = R_{s/p}\Delta E_p \tag{15}$$

with $R_{s/p}$ taken as the mean of the ratios for each station. Thus, using equation (12) with $V = h_0 r_0 w_0$, the volume of a granular flow as a function of its seismic energy is assumed to be

$$V = \frac{3E_s}{R_{s/p}\rho g L(\tan\alpha\cos\theta - \sin\theta)} \tag{16}$$

where the density $\rho = c_o\rho_i$, with $\rho_i = 2000$ kg m^{-3}, equal to the density of intact rock, and $c_o = 0.6$ the volume fraction of the solid material. Value of $L = 500$ m was chosen for the approximate slope length. The value of the mean angle of the slope $\theta = 35°$ was chosen from the friction coefficient δ estimated through simulations. In a range of realistic values, a variation of θ of 1° results in a variation of less than 0.5% of the total volume. Given that the flow is stopped by the floor of the crater, the deposit along the slope is almost parallel to the crater wall and consequently the mean angle α of the deposit is quasi-null, i.e., $\alpha = 0$.

[38] Figure 10 shows histograms of the computed volume distribution with a volume discretization of 100 m^3, and Table 2 gives monthly extreme and mean volume values for each station. The volumes range from 10 to 10^4 m^3: 80% of the events have a volume less than 1000 m^3, 67% a volume below 500 m^3 and 29% a volume below 100 m^3. The average cumulative volume calculated using the four stations is 1.85 Mm^3 with a standard deviation of 0.28 Mm^3. This volume corresponds to a deposit which covers the crater floor to a thickness of approximately 20 m. In comparison, the volume of the 1995 Mahavel rockfall episode involved 10 Mm^3 [*Rousseau*, 1999]. The cumulative volume computed using these methods seem to be fairly realistic considering the highly fractured geological context of Dolomieu crater and the time period studied (10 months).

5.3. Validation: The 16 May 2007 Rockfall

[39] On 16 May 2007 at 05:20 local time (LT), a major rockfall occurred in the southwest part of Dolomieu crater. The event was recorded by the OVPF seismological network and photographs taken before and after make it possible to identify its source area (Figures 11a and 11b) and its initial volume, which was estimated at about 5.8×10^4 m^3. The seismic energy of the rockfall, computed from the seismograms recorded at station BOR, was 2.3×10^8 J. The potential energy difference of this event, estimated from a 3-D simulation made with the SHALTOP model (Figures 11c and 11d), is 2.4×10^{11} J. Consequently the $E_s/\Delta E_p$ ratio is 9×10^{-4}. This value is within the range of those determined for the 1706 rockfall events analysis in section 5.1. The computed volume using equation (16) for this event is 8.3×10^4 m^3. The parameter values used for equation (16) were those of section 6.2, except for the average slope angle θ for which we used 60 degrees to better account for the steepness of the path taken by the fragments. The estimated volume and computed volume are quite close, considering the possible errors in the estimation made from the photographs and the choice of the average slope angle. This supports the use of equation (16) for computing rockfall volumes in our specific context and in the framework of the assumptions made in sections 4 and 5. However the robustness of our method and results can only be assessed through more observations of further granular flows with a precise estimation of their volumes and durations for comparison with the associated seismic signals. Seismic source mechanisms are another important aspect that needs to be addressed in order to better understand the relationships between the properties of rockfalls and their seismic signals.

6. Discussion: Temporal Variations of Rockfall Activity in Dolomieu Crater

[40] In section 5, we established the link between seismic energy and rockfall volumes. This section focuses on the temporal variations of the observed seismic energy and signal duration related to rockfall activity over the period 1 May 2007 to 28 February 2008 and some possible interpretations of the evolution of Dolomieu crater structure after the 6 April 2007 crater floor collapse.

[41] Figure 12a shows that rockfall activity was not constant within any month but rather concentrated in several pulses, indicating a temporal clustering of these events. The number of rockfalls in Dolomieu crater was highest just after the collapse (Figure 12a) with 489 events identified in May, and lowest in January 2008, with 55 events. A 30 day long window was used to compute a moving average of the total seismic energy, the mean seismic energy per event and mean duration as a function of time.

[42] The mean duration of the rockfalls (Figure 12b) exhibits a high variability and is hard to interpret. Signal durations are longer at stations DSR and BOR. This may be due to the difference of the seismic signal-to-noise ratio (SNR) because of station distances from the events. The SNR is better for stations BOR and DSR, which are closer to the seismic sources, explaining why mean duration is higher for these two stations. The maximum difference between the mean durations at different stations occurred in July 2007 with a value of 3.7 s. The mean standard deviation of the

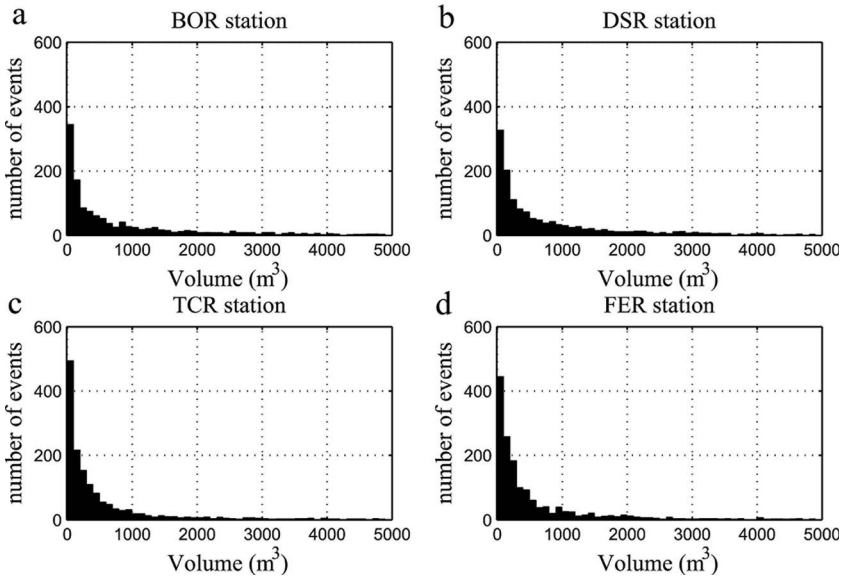

Figure 10. Histograms of the volume distribution of rockfalls estimated from seismic signals at the four seismic stations: (a) station BOR, (b) station DSR, (c) station TCR, and (d) station FER.

values of the average duration per month computed for the four stations is 2.2 s.

[43] The highest-energy production related to rockfall activity was observed in May 2007 just after the collapse (Figure 12c). By July 2007, the summed signal energy stabilized after which an average of 110 events per month occurred. On the basis of the mean value of the summed energy for each of the four stations, the total energy produced by the detected rockfalls in May and June 2007 was 1×10^9 J, whereas the total energy produced for the whole period studied was 1.25×10^9. Thus 80% of the observed energy released over the period of study was produced by rockfalls that occurred within two months of the crater floor collapse. If we limit the analysis to the May 2007 to November 2007 period, this value become 89%. In comparison, *Staudacher et al.* [2009] showed that 95% of the deflation of the volcano following crater floor collapse occurred by the end of June 2007, with an additional 5% between July and November 2007. Consequently, there is indeed a link between rockfall activity (volume and frequency of occurrence) and the crater deformation during the post-collapse period studied.

[44] The temporal trend in mean seismic energy per rockfall event (Figure 12d) is similar to that of total seismic energy produced by the rockfalls. However, the mean energy per event increased after November 2007 and was particularly high in February 2008. Réunion Island is subject to intense bouts of rainfall, with the rainy season extending from December to March and peak monthly precipitation in February. Several authors have shown that rainfall can increase the occurrence of rockfalls [*Helmstetter and Garambois*, 2010], trigger landslides [*Guzzetti et al.*, 2007] or in a volcanic context, can favor lava dome collapse [*Matthews et al.*, 2002]. To investigate a possible relationship between rainfall and rockfall occurrence, we compared the daily recorded rainfall and daily seismic energy calculated from the rockfall seismic signals at station DSR (Figure 13). The rainfall data (only available since mid-June 2007) were recorded at a station near the summit of the Piton de la Fournaise volcano.

[45] Isolated peaks of rockfall activity are probably spontaneous episodes provoked by the residual weakness of the crater edges. Nevertheless, several rockfall episodes do seem to be correlated to some peaks of rainfall (indicated by arrows in Figure 13) although without any apparent

Table 2. Sum of the Computed Volume of Rockfalls per Month and Extreme Values[a]

	BOR			DSR			TCR			FER		
	$\sum V$	V_{min}	V_{max}	$\sum V$	V_{min}	V_{max}	$\sum V$	V_{min}	V_{max}	$\sum V$	V_{min}	V_{max}
May 2007	910,635	6	20,447	851,719	11	14,088	1,088,911	16	67,414	1,072,552	63	32,354
June 2007	525,715	5	22,922	235,273	4	10,756	423,552	11	44,838	162,017	12	9,378
July 2007	119,826	3	1,1219	95,054	1	8,742	61,466	10	15,528	53,784	26	4,739
August 2007	59,681	5	7,092	48,916	5	3,382	35,953	15	2420	43,595	11	2,012
September 2007	82,538	8	9,011	48,256	6	3,112	34,112	13	2023	28,358	18	1,800
October 2007	116,742	7	12,867	65,393	3	4,594	107,434	17	63,283	36,789	16	2,461
November 2007	62,052	2	9,180	65,773	1	4,843	56,587	7	5758	81,206	24	8,675
December 2007	91,814	18	15,017	92,398	20	9,544	71,080	23	23,115	46,037	21	3,945
January 2008	85,486	23	12,379	51,945	37	11,915	31,227	33	5311	14,314	25	1,282
February 2008	162,085	32	20,869	130,497	47	8,513	148,356	39	32,769	72,241	36	7,551

[a]Total volumes for BOR, DSR, TCR, and FER are 2,216,578, 1,685,228, 2,058,682, and 1,610,849, respectively. Units are cubic meters (m^3).

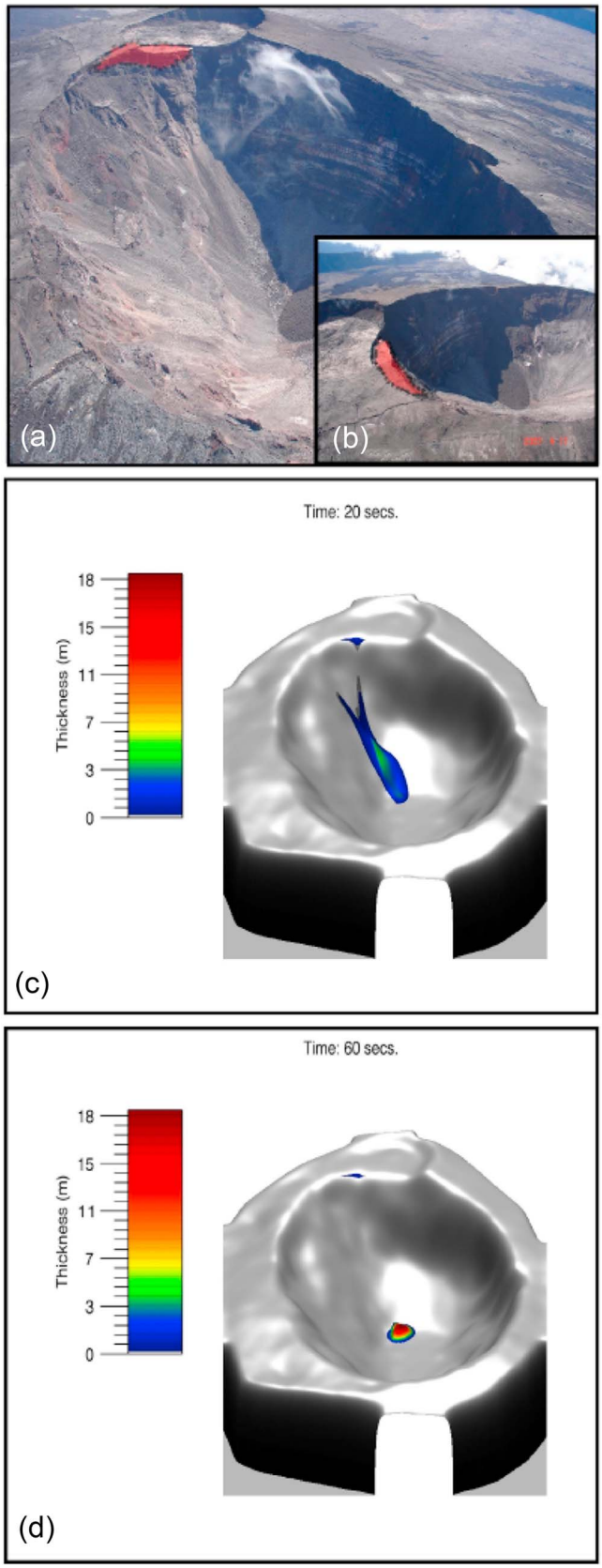

triggering threshold. Our analysis suggests that rainfall played a major role in the initiation of intense rockfall activity recorded in February 2008. In all but two cases (peaks appearing at the ends of November 2007 and February 2008), rockfall activity appears to start during a bout of heavy rainfall, mostly few hours after its beginning. This correlation of rockfall activity with rainfall might be explained by the extremely fractured nature of Dolomieu crater edges enabling fast and intense water infiltration. However, no quantitative correlation is found between rainfall intensity and the amount of seismic energy produced; intense bouts of rainfall did not systematically induce a period of high rockfall production.

[46] From all the information gathered we can build a picture of the rockfall activity within the period studied. Following crater floor collapse, crater deflation and highly destabilized crater edges favored numerous rockfalls covering a broad energy band but dominated by high-energy events and thus high volumes. Some short-duration events, probably characterized by a more prominent free-fall phase are also observed. This period of frequent rockfall activity which we call the crater relaxation period, appears to have ended by July 2007 when a stable level in both number of events and energy production was reached. Starting around December 2007 during the rainy season, rockfalls became less frequent but far more energetic, possibly as a result of environmental forcing on the metastable state of the crater edges. Large rainfall-initiated events during this period may have purged the unstable zones of the crater edges which otherwise might have produced smaller but more numerous rockfalls. However, the correlation between rainfall and rockfall occurrence is not systematic. The temporal variations of the seismological properties of rockfalls suggest that both crater deformation and rainfall affected rockfall activity. Determining a reference level for identifying rockfall episodes due to extraordinary conditions is important for assessing links between rockfall activity and volcano deformation related to eruptive periods.

7. Conclusion

[47] An approach combining seismic signal processing and numerical simulations of granular flows has been used to characterize rockfalls affecting Dolomieu crater at Piton de la Fournaise volcano. Seismic signal processing techniques made it possible to distinguish rockfall signals from other events recorded by the OVPF seismological network. Moreover, these techniques proved useful to distinguish granular flow from the free-fall rockfalls, and to identify the predominant source mechanisms in the seismic signals. We deduced that detachment of rock masses and their subsequent impact accounted for most of the seismic signals generated by free-fall-type rockfalls, but that flow dominated signals associated with granular flows.

Figure 11. (a) Photograph from the east side of the Dolomieu crater showing the mass that detached on 16 May 2007; (b) close-up view of the mass from south of the Dolomieu crater. (c) The 3-D simulation of the rockfall at time t = 20 s: the mass is spreading along the slope. (d) The 3-D simulation of the rockfall at time t = 60 s: the mass has formed the final deposit.

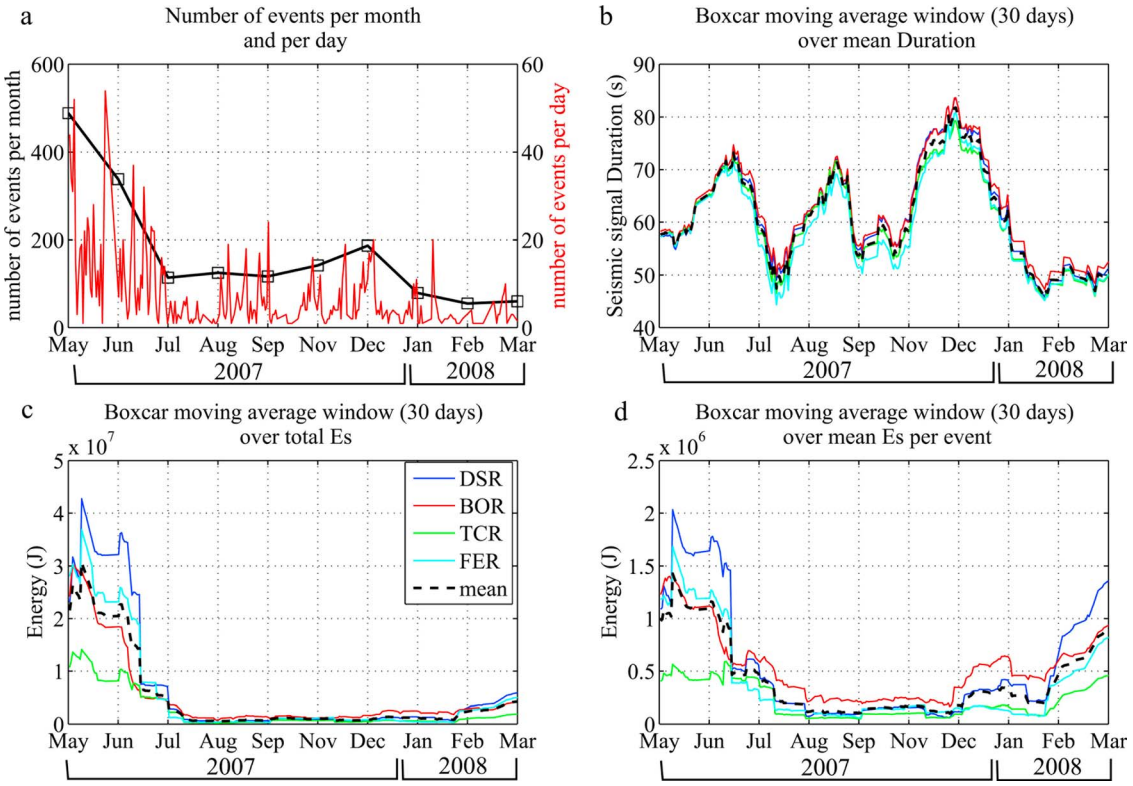

Figure 12. (a) Number of events per month (black) and per day (red), (b) mean duration of granular flow seismic signal for stations BOR, DSR, TCR, and FER and global average values (black line), (c) sum of the seismic energy produced by granular flows per month and for stations BOR, DSR, TCR, and FER and global average values (black line), and (d) mean seismic energy per event per month and for stations BOR, DSR, TCR, and FER and global average values (black line).

[48] The similar trends between the scaling laws that we have found, relating seismic energy and potential energy to duration, suggest a linkage between the seismic and potential energy involved in a given granular flow. The computed ratio of seismic to potential energy indicates that the quantity of energy dissipated in the form of seismic waves is a small fraction (10^{-4}) of the potential energy released. An analytical approach based on theoretical and experimental work on granular material flowing over inclined planes, provided us with a way of assessing rockfall mass on a physical basis and determining the volume of an event from the seismic energy. These developments thus provide a simple methodology based on physical modeling of rockfalls to trace back their volumes from the associated seismic

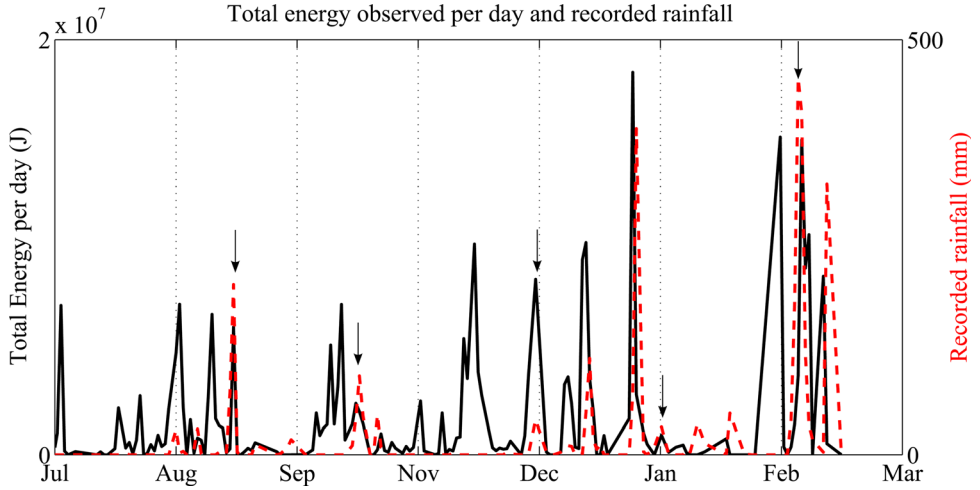

Figure 13. Seismic energy (black) at DSR station and recorded rainfall (dashed red line).

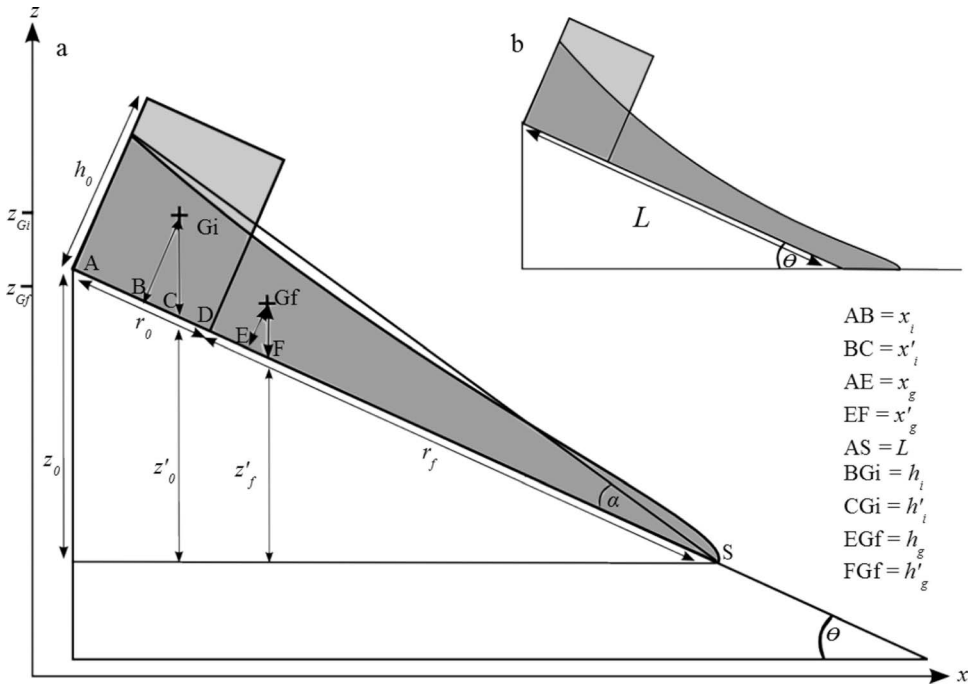

Figure A1. (a) Initial and final positions of a granular flow with a finite initial mass with a rectangular shape released on a flat slope. *Gi* and *Gf* are the positions of the initial and the final mass centers, respectively. Normal projection with respect to the slope of the horizontal distance between centers of mass and the slope top are x_i and x_g for the initial and final states, respectively. Normal projection with respect to the horizontal axis x of the horizontal distance between centers of mass and the slope top are x'_i and x'_g for the initial and final states, respectively. Here $z'_0 + h'_i$ is the height difference between the initial mass center position (*Gi*) and the ending position (*S*) reached by the spreading mass, $z'_f + h'_g$ is the height difference between the final mass center position (*Gf*) and the ending position (*S*) reached by the spreading mass, and h_i and h_g are the heights with respect to the slope of the initial and final mass centers, respectively. (b) The same case as in Figure A1a but with the mass halted by the topography.

signal. The methodology presented here may be used in different geological context for a real-time volume estimation of rockfalls. Moreover, a remote study of the rockfall activity using this method can provide important statistical data that may lead to a better hazards assessment.

[49] Our results reveal a temporal link between deflation of the Piton de la Fournaise summit, following Dolomieu crater floor collapse, and the rockfall activity. Furthermore, rainfall appears to have influenced the occurrence of rockfalls, but we find no correlation between rainfall intensity, rainfall amount, and generated seismic energy. This demonstrates that the study of the rockfall activity may provide interesting information on the evolution of large destabilized structure, such as volcano crater, and could be of interest in our case for further investigations of data provided during eruptive periods.

Appendix A: Detail of the Analytical Solution for an Inclined Bed

[50] Using the parameters defined in Figure A1a, the initial position of the granular mass center can be computed as follows:

$$z_{Gi} = z'_0 + h'_i \tag{A1}$$

Because $\cos\theta = \frac{h_i}{h'_i}$ and $h_i = \frac{h_0}{2}$, we obtain

$$h'_i = \frac{h_0}{2\cos\theta} \tag{A2}$$

[51] Furthermore, $\sin\theta = \frac{z'_0}{L - \frac{r_0}{2} - x'_i} = \frac{z_0}{L}$ and $x'_i = h_i \tan\theta$; hence,

$$z'_0 = \sin\theta\left(L - \frac{r_0}{2} - h_i\tan\theta\right) \tag{A3}$$

which leads to

$$z'_0 = z_0 - \sin\theta\left(\frac{r_0}{2} - \frac{h_0}{2}\tan\theta\right) \tag{A4}$$

The altitude of the initial mass center position can be obtained from equations (A1), (A2), and (A4):

$$z_{Gi} = z_0 - \sin\theta\left(\frac{r_0}{2} + \frac{h_0}{2}\tan\theta\right) + \frac{h_0}{2\cos\theta} \tag{A5}$$

The final altitude of the mass center is given by

$$z_{Gf} = z'_f + z'_g \tag{A6}$$

Using $\cos\theta = \frac{z_g}{z'_g}$ and the definition of the mass center of a right-angled triangle, we obtain ($z_g = \frac{R_f \tan\alpha}{3}$, $x_g = \frac{R_f}{3}$) with $R_f = r_0 + r_f$, so

$$z'_g = \frac{R_f \tan\alpha}{3\cos\theta} \tag{A7}$$

Moreover, $\sin\theta = \frac{z'_f}{L - x_G - x'_G} = \frac{z'_f}{L - x_G - z_G \tan\theta}$, so

$$z'_f = \sin\theta\left(L - \frac{R_f}{3} - \frac{R_f \tan\alpha}{3}\tan\theta\right)$$

$$z'_f = z_0 - \frac{\sin\theta}{3}R_f(1 + \tan\alpha\tan\theta) \tag{A8}$$

Finally, from equations (A6), (A7), and (A8) the final altitude of the mass center can be expressed as

$$z_{Gf} = z_0 - \frac{R_f \sin\theta}{3}(1 + \tan\alpha\tan\theta) + \frac{R_f \tan\alpha}{3\cos\theta} \tag{A9}$$

[52] From equations (6), (A5), and (A9) we can express the difference of potential energy as follows:

$$\Delta E_p = mg\left[\frac{-R_f \sin\theta}{3}(1 + \tan\alpha\tan\theta) + \frac{R_f \tan\alpha}{3\cos\theta} + \sin\theta\left(\frac{r_0}{2} + \frac{h_0}{2}\tan\theta\right) - \frac{h_0}{2\cos\theta}\right] \tag{A10}$$

[53] Replacing R_f, we obtain

$$\Delta E_p = mg\left\{r_f\left[\frac{-\sin\theta}{3}(1 + \tan\ \alpha\tan\theta) + \frac{\tan\alpha}{3\cos\theta}\right] + r_0\left[\frac{-\sin\theta}{3}(1 + \tan\alpha\tan\theta) + \frac{\tan\alpha}{3\cos\theta} + \frac{\sin\theta}{2}\right] + h_0\left(\frac{\sin^2\theta - 1}{2\cos\theta}\right)\right\} \tag{A11}$$

so

$$\Delta E_p = mg\left\{r_f\left(\frac{-\sin\theta}{3} - \frac{\tan\alpha\sin^2\theta}{3\cos\theta} + \frac{\tan\alpha}{3\cos\theta}\right) + r_0\left[\left(\frac{-\sin\theta}{3} - \frac{\tan\alpha\sin^2\theta}{3\cos\theta} + \frac{\tan\alpha}{3\cos\theta}\right) + \frac{\sin\theta}{2}\right] - \left(\frac{h_0\cos\theta}{2}\right)\right\} \tag{A12}$$

$$\Delta E_p = mg\left(r_f\left[\frac{-\sin\theta}{3} + \frac{\tan\alpha}{3}\left(\frac{1 - \sin^2\theta}{\cos\theta}\right)\right] + r_0\left\{\left[\frac{\tan\alpha}{3}\left(\frac{1 - \sin^2\theta}{\cos\theta}\right)\right] + \frac{\sin\theta}{6}\right\} - \left(\frac{h_0\cos\theta}{2}\right)\right) \tag{A13}$$

The change in potential energy of a granular flow on a flat slope can therefore be expressed as

$$\Delta E_p = mg\left[\frac{-h_0\cos\theta}{2} + \frac{1}{3}(\tan\alpha\cos\theta - \sin\theta)r_f + \frac{1}{3}\left(\tan\alpha\cos\theta + \frac{\sin\theta}{2}\right)r_0\right] \tag{A14}$$

[54] **Acknowledgments.** This study is part of the UNDERVOLC project and is supported by grants from the French Agence Nationale de la Recherche (ANR) and BRGM. We are very grateful to the UNDERVOLC team and members of the Observatoire du Piton de la Fournaise, particularly, Valerie Ferrazini, Andrea DiMuro, Thomas Staudacher, Florent Brenguier, and Elodie Rivemale, for their useful discussions and support in the field. We also thank Agnès Helmstetter and Jean Robert Grasso for interesting discussions. The authors gratefully acknowledge E. S. Calder, W. Thelen, and an anonymous reviewer for helpful reviews. We would like to thank the editors for their substantial work, which helped to greatly improve the manuscript.

References

Aki, K., and P. G. Richards (1980), *Quantitative Seismology: Theory and Methods*, 2nd ed., 645 pp., Univ. Sci. Books, Sausalito, Calif.

Bessason, B., G. Eiriksson, O. Thorarinsson, A. Thorarinsson, and S. Einarsson (2007), Automatic detection of avalanches and debris flows by seismic methods, *J. Glaciol.*, *53*, 461–472.

Börzsönyi, T., T. C. Halsey, and R. E. Ecke (2008), Avalanche dynamics on a rough inclined plane, *Phys. Rev. E*, *78*, 011306.

Bouchut, F., and M. Westdickenberg (2004), Gravity driven shallow water models for arbitrary topography, *Commun. Math. Sci.*, *2*, 359–389.

Bouchut, F., A. Mangeney-Castelnau, B. Perthame, and J. P. Vilotte (2003), A new model of Saint-Venant and Savage-Hutter type for gravity driven shallow water flows, *C. R. Acad. Sci. Paris, Ser. I*, *336*, 531–536.

Brenguier, F., N. M. Shapiro, M. Campillo, A. Nercessian, and V. Ferrazzini (2007), 3-D surface wave tomography of the Piton de la Fournaise volcano using seismic noise correlation, *Geophys. Res. Lett.*, *34*, L02305, doi:10.1029/2006GL028586.

Calder, E. S., R. Luckett, R. S. J. Sparks, and B. Voight (2002), Mechanisms of lava dome instability and generation of rockfalls and pyroclastic flows at Soufrière Hills volcano, Montserrat, in *The Eruption of Soufrière Hills Volcano, Montserrat, From 1995 to 1999*, edited by T. H. Druitt and B. P. Kokelaar, *Geol. Soc. London Mem.*, *21*, 483–516.

Calder, E. S., J. A. Cortes, J. L. Palma, and R. Luckett (2005), Probabilistic analysis of rockfall frequencies during an andesite lava dome eruption: The Soufrière Hills volcano, Montserrat, *Geophys. Res. Lett.*, *32*, L16309, doi:10.1029/2005GL023594.

Dahlen, F. (1993), Single-force representation of shallow landslide sources, *Bull. Seismol. Soc. Am.*, *83*, 130–143.

Deparis, J., D. Jongmans, F. Cotton, L. Baillet, F. Thouvenot, and D. Hantz (2007), Analysis of rock-fall seismograms in the western Alps, *Bull. Seismol. Soc. Am.*, *98*, 1781–1796.

Eissler, H. K., and H. Kanamori (1987), A single-force model for the 1975 Kalapana, Hawaii, earthquake, *J. Geophys. Res.*, *92*, 4827–4836.

Favreau, P., A. Mangeney, A. Lucas, G. Crosta, and F. Bouchut (2010), Numerical modeling of landquakes, *Geophys. Res. Lett.*, *37*, L15305, doi:10.1029/2010GL043512.

Ferrazzini, V., K. Aki, and B. Chouet (1991), Characteristics of seismic waves composing Hawaiian volcanic tremor and gas-piston events observed by a near source array, *J. Geophys. Res.*, *96*, 6199–6209.

Fukushima, Y., V. Cayol, and P. Durand (2005), Finding realistic dike models from interferometric synthetic aperture radar data: The February 2000 eruption at Piton de La Fournaise, *J. Geophys. Res.*, *110*, B03206, doi:10.1029/2004JB003268.

Guzzetti, F., S. Peruccacci, M. Rossi, and C. P. Stark (2007), Rainfall thresholds for the initiation of landslides in central and southern Europe, *Meteorol. Atmos. Phys.*, *98*, 239–267, doi:10.1007/s00703-007-0262-7.

Helmstetter, A., and S. Garambois (2010), Seismic monitoring of Séchilienne rockslide (French Alps): Analysis of seismic signal and their correlation with rainfalls, *J. Geophys. Res.*, *115*, F03016, doi:10.1029/2009JF001532.

Hibert, C., T. Dewez, A. Mangeney, G. Grandjean, P. Boissier, P. Catherine, and P. Kowalski (2010), Rockfall photogrammetric monitoring in the active crater of Piton de la Fournaise volcano, La Reunion Island, *Geophys. Res. Abstr.*, *12*, Abstract EGU2010-6928.

Kanamori, H., and J. W. Given (1982), Analysis of long-period seismic waves excited by the May 18, 1980, eruption of Mount St. Helens—A terrestrial monopole?, *J. Geophys. Res.*, *87*, 5422–5432.

Koyanagi, S., K. Mayeda, and K. Aki (1992), Frequency dependent site amplification factors using the S-waves coda for the island of Hawaii, *Bull. Seismol. Soc. Am.*, *82*, 1151–1185.

Kuo, C. Y., Y. C. Tay, F. Bouchut, A. Mangeney, M. Pelanti, R. F. Chen, and K. J. Chang (2009), Simulation of Tsaoling landslide, Taiwan, based on Saint Venant equations over general topography, *Eng. Geol.*, *104*(3–4), 181–189.

Leonard, M., and B. L. N. Kennett (1998), Multi-component autoregressive techniques for the analysis of seismograms, *Phys. Earth Planet. Inter.*, *113*, 247–263.

Lucas, A., and A. Mangeney (2007), Mobility and topographic effects for large Valles Marineris landslides on Mars, *Geophys. Res. Lett.*, *34*, L10201, doi:10.1029/2007GL029835.

Lucas, A., A. Mangeney, D. Mège, and F. Bouchut (2011), Influence of the scar geometry on landslide dynamics and deposits: Application to Martian landslides, *J. Geophys. Res.*, *116*, E10001, doi:10.1029/2011JE003803.

Luckett, R., E. Baptie, and J. Neuberg (2002), The relationship between degassing and rockfall signals at Soufrière Hills Volcano, Montserrat, *Geol. Soc. London Mem.*, *21*, 565–602.

Mangeney, A., P. Heinrich, R. Roche, G. Boudon, and J. L. Cheminée (2000), Modeling of debris avalanche and generated water waves: Application to real and potential events in Montserrat, *Phys. Chem. Earth.*, *25*(9–11), 741–745.

Mangeney, A., L. S. Tsimring, D. Volfson, I. S. Aranson, and F. Bouchut (2007), Avalanche mobility induced by the presence of an erodible bed and associated entrainment, *Geophys. Res. Lett.*, *34*, L22401, doi:10.1029/2007GL031348.

Mangeney, A., O. Roche, O. Hungr, N. Mangold, G. Faccanoni, and A. Lucas (2010), Erosion and mobility in granular collapse over sloping beds, *J. Geophys. Res.*, *115*, F03040, doi:10.1029/2009JF001462.

Mangeney-Castelnau, A., F. Bouchut, J. P. Vilotte, E. Lajeunesse, A. Aubertin, and M. Pirulli (2005), On the use of Saint-Venant equations to simulate the spreading of a granular mass, *J. Geophys. Res.*, *110*, B09103, doi:10.1029/2004JB003161.

Mangold, N., A. Mangeney, V. Migeon, V. Ansan, A. Lucas, D. Baratoux, and F. Bouchut (2010), Sinuous gullies on Mars: Frequency, distribution, and implications for flow properties, *J. Geophys. Res.*, *115*, E11001, doi:10.1029/2009JE003540.

Matthews, A. J., J. Barclay, S. Carn, G. Thompson, J. Alexander, R. Herd, and C. Williams (2002), Rainfall-induced volcanic activity on Montserrat, *Geophys. Res. Lett.*, *29*(13), 1644, doi:10.1029/2002GL014863.

McNutt, S. R. (1996), Seismic monitoring and eruption forecasting of volcanoes: A review of the state-of-the-art and case histories, in *Monitoring and Mitigation of Volcano Hazards*, edited by R. Scarpa and R. Tilling, pp. 99–146, Springer, Berlin.

Michon, L., T. Staudacher, V. Ferrazzini, P. Bachelery, and J. Marti (2007), April 2007 collapse of Piton de la Fournaise: A new example of caldera formation, *Geophys. Res. Lett.*, *34*, L21301, doi:10.1029/2007GL031248.

Norris, R. D. (1994), Seismicity of rockfalls and avalanches at three cascade range volcanoes: Implications for seismic detection of hazardous mass movements, *Bull. Seismol. Soc. Am.*, *84*, 1925–1939.

Peltier A., T. Staudacher, and P. Bachelery (2007), Constraints on magma transfers and structures involved in the 2003 activity at Piton de La Fournaise from displacement data, *J. Geophys. Res.*, *112*, B03207, doi:10.1029/2006JB004379.

Ratdomopurbo, A., and G. Poupinet (2000), An overview of the seismicity of Merapi volcano (Java, Indonesia), 1983–1994, *J. Volcanol. Geotherm. Res.*, *100*, 193–214.

Rousseau, N. (1999), Study of seismic signal associated with rockfalls at 2 sites on the Réunion Island (Indian Ocean): Mahavel Cascade and Soufrière cavity, Ph.D. thesis, 134 pp., Inst. de Phys. du Globe de Paris, Paris.

Staudacher, T., V. Ferrazzini, A. Peltier, P. Kowalski, P. Boissier, P. Catherine, F. Lauret, and F. Massin (2009), The April 2007 eruption and Dolomieu crater collapse, two major events at Piton de la Fournaise (La Réunion Island), *J. Volcanol. Geotherm. Res.*, *184*, 126–137.

Surinach, E., I. Vilajosana, B. Khazaradze, B. Biescas, G. Furdada, and J. M. Vilaplana (2005), Seismic detection and characterization of landslides and other mass movements, *Nat. Hazards Earth Syst. Sci.*, *5*, 791–798.

Urai, M., N. Geshi, and T. Staudacher (2007), Size and volume evaluation of the caldera collapse on Piton de la Fournaise volcano during the April 2007 eruption using ASTER stereo imagery, *Geophys. Res. Lett.*, *34*, L22318, doi:10.1029/2007GL031551.

Vilajosana, I., E. Surinach, A. Abellan, G. Khazaeadze, D. Garcia, and J. Llosa (2008), Rockfall induced seismic signal: Case study in Montserrat, Catalonia, *Nat. Hazards Earth Syst. Sci.*, *8*, 805–812.

Zobin, V. M. (2003), *Introduction to Volcanic Seismology*, vol. 6, 290 pp., Elsevier, Amsterdam.

Zobin, V. M., N. R. Varley, M. Gonzalez, J. Orzco, G. A. Reyes, C. Navarro, and M. Breton (2008), Monitoring the 2004 andesitic block-lava extrusion at Volcan de Colima, Mexico from seismic activity and SO_2 emission, *J. Volcanol. Geotherm. Res.*, *177*, 367–377.

G. Grandjean, Bureau des Recherches Géologiques et Minières, RNSC/RMT, 3 avenue Claude-Guillemin, BP 36009, F-45060 Orléans CEDEX 2, France. (g.grandjean@brgm.fr)

C. Hibert, A. Mangeney, and N. M. Shapiro, Institut de Physique du Globe de Paris, Equipe de Sismologie, Université Paris Diderot–Paris 7, 4 place Jussieu, F-75252 Paris CEDEX 05, France. (hibert@ipgp.fr; mangeney@ipgp.jussieu.fr)